Imaging of Delayed-Type Hypersensitivity Reaction by PET and ^{18}F-Galacto-RGD

Bernd J. Pichler, PhD[1]; Manfred Kneilling, MD[2]; Roland Haubner, PhD[1]; Heidi Braumüller, PhD[2]; Markus Schwaiger, MD[1]; Martin Röcken, MD[2]; and Wolfgang A. Weber, MD[1]

[1]*Nuklearmedizinische Klinik und Poliklinik, Klinikum rechts der Isar, Technische Universität München, München, Germany; and* [2]*Department of Dermatology, University Tübingen, Tübingen, Germany*

Radiolabeled cyclic peptides containing the amino acid sequence arginine-glycine-aspartate (RGD peptides) have successfully been used to image the expression of the $\alpha_v\beta_3$ integrin in malignant tumors. However, the $\alpha_v\beta_3$ integrin also plays an important role in angiogenesis induced by chronic inflammatory processes. Therefore, the aim of this study was to evaluate whether radiolabeled RGD peptides may also be used to assess $\alpha_v\beta_3$ expression in inflammatory diseases. We studied a hapten-induced delayed-type hypersensitivity reaction (DTHR) as a model for inflammatory processes, since DTHRs are involved in many human autoimmune disorders. **Methods:** The abdominal skin of mice was sensitized by application of 2,4,6-trinitrochlorobenzene (TNCB). One week later, a DTHR was elicited by challenging the right ear with TNCB. Application of TNCB was then repeated every 48 h to induce chronic skin inflammation. Small-animal PET and autoradiography with the $\alpha_v\beta_3$ ligands ^{18}F-galacto-RGD and ^{125}I-gluco-RGD were performed at various times after TNCB application. The time course of tracer uptake by the treated ears was compared with histologic skin changes. **Results:** The first challenge with TNCB caused, within 12 h, an acute inflammatory response with dense dermal infiltrates of polymorphonuclear leukocytes and lymphocytes. However, autoradiography revealed no significant increase in ^{125}I-gluco-RGD uptake at that time (mean uptake ratio for treated ear to untreated ear, 1.02 ± 0.1 [SD]). Further challenges with TNCB resulted in chronic skin inflammation with markedly increased small-vessel density in the ear tissue. This was paralleled by a continuous increase in uptake of ^{125}I-gluco-RGD. After 13 challenges, the uptake ratio had increased to 2.30 ± 0.27 ($P < 0.005$ compared with baseline). Enhanced uptake of radiolabeled RGD peptides in chronic inflammation was also demonstrated noninvasively by PET with ^{18}F-galacto-RGD. Pretreatment of the mice with nonradiolabeled cyclic peptide c(RGDfV) almost completely blocked uptake of ^{18}F-galacto-RGD by the challenged ear, thus confirming the specificity of tracer uptake. **Conclusion:** Radiolabeled RGD peptides allow a noninvasive assessment of $\alpha_v\beta_3$ expression in inflammatory processes. PET with ^{18}F-galacto-RGD might become a powerful tool to distinguish between the acute and chronic phases of T cell–mediated immune responses and may represent a new biomarker for disease activity in autoimmune disorders.

Key Words: autoradiography; molecular imaging; PET; radiopharmaceuticals; animal imaging; inflammation

J Nucl Med 2005; 46:184–189

Integrins, a large family of cell adhesion molecules, are the main mediators of the binding and response of cells to the extracellular matrix. Each integrin is composed of 2 noncovalently associated transmembrane glycoprotein subunits called the α- and the β-chains. So far, 18 α- and 8 β-chains have been identified, which form at least 24 receptors with different substrate specificities (*1*). One of the best characterized of these receptors is the $\alpha_v\beta_3$ integrin, which plays an important role for endothelial cell migration and survival during angiogenesis. In contrast, $\alpha_v\beta_3$ is found only in minimal amounts in resting endothelial cells. Tumor cells of various origins, particularly melanomas, can also express $\alpha_v\beta_3$. In normal tissues, expression of $\alpha_v\beta_3$ is highly restricted, and significant amounts of this integrin have been observed only in osteoclasts (*2*). This limited expression by normal tissues makes $\alpha_v\beta_3$ a particularly attractive target for imaging probes.

The binding mechanisms of $\alpha_v\beta_3$ integrin to its ligands (e.g., vitronectin, fibronectin, fibrinogen, and osteopontin) have been studied extensively in recent years (*3*). It is now well established that $\alpha_v\beta_3$ binds to matrix proteins with an exposed RGD (arginine-glycine-aspartate) sequence (*4*). This binding motif is also used by several other integrin subtypes (e.g., $\alpha_v\beta_5$ and $\alpha_{IIb}\beta_3$) (*3*). However, the binding affinity of different integrins to proteins containing an RGD motif is critically influenced by the 3-dimensional arrangement of the 3 amino acids in this sequence as well as by the flanking amino acid residues (*3*). Intensive structure/activity investigations have resulted in the development of cyclic pentapeptides that specifically bind to $\alpha_v\beta_3$ but not to other related RGD-binding integrins (*5*). Radiolabeling of these peptides with radioiodine, ^{111}In, ^{99m}Tc, and ^{18}F, has allowed the development of various imaging agents that specifically localize to tumors expressing $\alpha_v\beta_3$ (*6*).

$\alpha_v\beta_3$ is also highly expressed in endothelial cells during wound healing (*7*), in restenosis after angioplasty (*8*), in the

Received Mar. 19, 2004; revision accepted Sep. 13, 2004.

For correspondence or reprints contact: Bernd J. Pichler, PhD, Department of Radiology, University of Tübingen, Hoppe-Seyler-Strasse 3, 72076 Tübingen, Germany.

E-mail: Bernd.Pichler@med.uni-tuebingen.de

synovia of patients with rheumatoid arthritis (*9*), and in psoriatic plaques (*10*). In an experimental model of rheumatoid arthritis, treatment with the cyclic RGD peptide c(RGDfV) significantly inhibited disease progression (*11*). Furthermore, $\alpha_v\beta_3$ antagonists have been shown to inhibit bone resorption by osteoclasts. Antibodies against $\alpha_v\beta_3$ or cyclic RGD peptides are, therefore, currently being evaluated as a new therapeutic approach for rheumatoid arthritis (*12*). Thus, radiolabeled RGD peptides may be used to characterize not only malignant tumors but also inflammatory diseases.

To evaluate uptake of radiolabeled RGD peptides by inflammatory processes, we studied a murine model for the cutaneous delayed-type hypersensitivity reaction (DTHR). We selected this model because DTHRs are involved in several common autoimmune disorders in humans, such as rheumatoid arthritis or chronic inflammatory bowel disease. In these diseases, DTHRs are directed against peptide antigens present within the tissues. However, cutaneous DTHR may also be induced by haptens applied to the skin. In our experiments, we used the hapten 2,4,6-trinitrochlorobenzene (TNCB) to induce contact hypersensitivity reactions (CHSRs), which have been well characterized in previous studies (*13,14*). In mice previously sensitized to TNCB, the first challenge with TNCB at one ear causes acute skin inflammation (acute CHSR), and the other, nontreated, ear is used as a control. Repeated challenges with TNCB result in chronic skin inflammation (chronic CHSR). Thus, this model allowed us to study the expression of $\alpha_v\beta_3$ in acute and chronic inflammation. As imaging probes, we used the glycosylated RGD peptides ^{125}I-gluco-RGD and ^{18}F-galacto-RGD. These peptides show almost the same affinity and specificity for the $\alpha_v\beta_3$ integrin. They also demonstrate a similar biodistribution in tumor-bearing mice (*15,16*). PET with ^{18}F-galacto-RGD has recently been shown to allow imaging of $\alpha_v\beta_3$ expression in patients with various malignant tumors (*17*). In the present study, ^{125}I-gluco-RGD was used for autoradiographic studies and ^{18}F-galacto-RGD for PET.

MATERIALS AND METHODS

Animals

All animal experiments were performed in accordance with the guidelines of the Technische Universität München for the use of living animals in scientific studies and the German Law for the Protection of Animals. The C57BL/6 mice (Charles River Laboratories) were between 8 and 12 wk old.

In Vivo Experiments

Mice were sensitized by application of 80 μL of 5% TNCB (dissolved in a 4:1 mixture of acetone and olive oil, w/w) to the shaved abdomen (size, ~2 × 2 cm). One week later, the mice were challenged with 20 μL of 1% TNCB (dissolved in a 1:9 mixture of acetone and olive oil, w/w) on both sides of the right ear, to elicit acute TNCB-specific CHSR. In the 5% TNCB solution acetone is an irritant, whereas it is used solely as a solvent in the 1% TNCB solution. To induce chronic cutaneous DTHR, mice (n = 3–6) were recurrently challenged at the ear every 2 d for a total of up to 13 challenges. Elicitation of CHSR at an ear allows easy assessment of the degree of inflammation through measurement of ear thickness with a micrometer (Oditest; Kroeplin) before the first TNCB challenge and 12 h after every subsequent ear challenge. TNCB was purchased from Fluka (Switzerland), ^{18}F was produced with an 11-MeV RDS cyclotron (CTI) at the Technische Universität München, and ^{125}I was purchased from Amersham-Buchler.

Synthesis of Gluco- and Galacto-RGD

^{125}I-gluco-RGD and ^{18}F-galacto-RGD were synthesized as described previously (*15,18*). Briefly, the linear peptides aspartate-tyrosine-lysine-arginine-glycine and aspartate-phenylalanine-lysine-arginine-glycine were assembled on solid support using standard 9-fluorenylmethoxycarbonyl (Fmoc) protocols and cyclized under high dilution conditions. Thereafter, they were conjugated with the benzylated glucose-based sugar amino acid Ac-SAA1(Bn_3)-OH (*15*) and Fmoc-protected galactose-based sugar amino acid Fmoc-SAA2-OH (*15*), respectively. ^{125}I-gluco-RGD was labeled with no-carrier-added ^{125}I-NaI by the IODO-GEN method (Pierce). The radiochemical purity as assessed by high-performance liquid chromatography was >95%, and the specific activity was >10 TBq/mmol. ^{18}F-galacto-RGD was labeled using no-carrier-added 4-nitrophenyl-2-^{18}F-fluoropropionate. The radiochemical purity of the final product was >98% as assessed by high-performance liquid chromatography, and the specific activity was >40 TBq/mmol (*15,18*).

Autoradiography

For digital phosphor storage autoradiography, 370 kBq of ^{125}I-gluco-RGD were intravenously injected into the tail vein and the animals were sacrificed 3 h afterward. During the uptake period, the mice were not kept anesthetized. Immediately after dissection, the ears were embedded in optimal cutting temperature compound (TissueTek; Fisher Scientific) and frozen in liquid nitrogen. Autoradiography was performed with the phosphor imager 445SI (Amersham Bioscience/Molecular Dynamics) from 20-μm fresh-frozen sections of the left, nonchallenged, and right, challenged, ears. Autoradiographic studies were performed on groups of 3–6 mice 12 h (time of animal scarification) after the first, second, fourth, eighth, tenth, and thirteenth challenges. Further autoradiograms were obtained for a group of 3 mice 24 h (time of animal scarification) after the first challenge to observe potential dynamic changes in tracer uptake at different times. The autoradiography data were analyzed with ImageQuant software (version 5.1; Molecular Dynamics). For each mouse rectangular regions of interest of the same size were drawn around 3 sections of the left and right ears. For further analysis, the mean value of the 3 autoradiograms per ear was used to calculate tracer uptake.

Histology and Immunohistochemistry

Histologic staining with hematoxylin and eosin was performed on 5-μm cryosections. In addition, vascular endothelial cells were stained with a platelet endothelial cell adhesion molecule-1 (PECAM-1, cluster designation 31 [CD31]) rat-antimouse antibody (BD Pharmingen) to allow visualization of vascularization. As a control antibody, rat-Igb2ακ (BD Pharmingen) was used. Staining was performed according to the instructions of the manufacturer.

High-Resolution Animal PET

PET was performed using the Munich Avalanche Diode PET (MADPET) (*19*), a prototype small-animal positron tomograph.

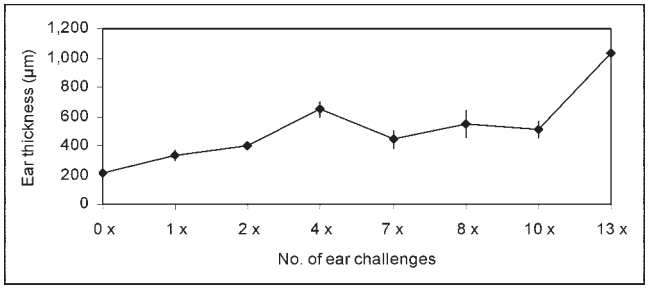

FIGURE 1. Time course of ear thickness 12 h after TNCB challenge. Error bars denote 1 SD.

The scanner consists of 2 sectors comprising 3 detector modules each, which rotate around the animal for acquisition of complete projections in 1 transaxial slice (30 angular steps). List-mode data are reconstructed using statistical, iterative methods including the spatially dependent line-spread function. Reconstructed image resolution is about 2.5 mm (full width at half maximum) in a transaxial field of view of about 5 cm. A 9.25-MBq aliquot of ^{18}F-galacto-RGD was injected into the tail vein 2 h before the 20-min PET scan. The animals were kept under anesthesia (intraperitoneal injection of 80 mg of Ketanest [Parke-Davis] and 10 mg of xylazine per kilogram of body weight) during scanning. MADPET has an axial field of view of only 3.7 mm; thus, the mice were scanned supine, with the neck gently flexed to the thorax so that only the ears were in the field of view. To estimate relative tracer uptake by the left and right ears, we manually drew regions of interest around both ears and calculated the ratio between mean counts for the right and left ears.

Statistical Analysis

All quantitative results are presented as the mean value ± SD. A *t* test result with a 2-tailed *P* value of less than 0.05 was considered statistically significant.

RESULTS

Morphologic Changes During Acute and Chronic Inflammation

Twelve hours after the first elicitation of acute cutaneous DTHR, there was edematous ear swelling, resulting in an increase of ear thickness from 210 ± 9 μm to 331 ± 37 μm ($P < 0.00001$) at the site of TNCB challenge. Repeated challenges at the ear caused TNCB-specific chronic inflammation, which was associated with a stepwise increase in ear thickness (Fig. 1). The average thickness of the treated ears increased from 210 ± 9 μm (no challenge) to 1,037 ± 81 μm (12 h after the 13th challenge) ($P < 0.003$ compared with baseline). Almost no signs of inflammation and no increase in ear thickness were found in ears from naïve mice treated once with TNCB, confirming that the inflammatory reaction was a TNCB-specific immune response (Fig. 2A).

Histologic examination of hematoxylin- and eosin-stained ear tissue 12 h after the first TNCB challenge of sensitized mice confirmed the presence of typical changes found in acute inflammatory responses, such as a dense dermal infiltration of polymorphonuclear leukocytes and lymphocytes, as well as the formation of subepidermal abscesses (Fig. 2B). Furthermore, extensive dilation of blood vessels and strong interstitial edema were found. In contrast, chronic TNCB-specific inflammation was associated with acanthosis, hyperkeratosis, and an increase of the number of new blood vessels, whereas the interstitial edema was less pronounced (Fig. 2C). PECAM-1 (CD31) immunohistochemistry confirmed the extensive neovascularization after the 10th challenge (Fig. 3).

RGD Peptides as Specific Markers for Chronic Inflammation

Twelve hours after the TNCB challenge, autoradiography demonstrated only a minimally increased uptake of ^{125}I-gluco-RGD in the challenged right ear, compared with the untreated left ear (Fig. 4). Quantitatively, the ratio of tracer uptake by the right and left ears was 1.03 ± 0.2 (P = not significant; Fig. 5). Tracer uptake also remained low at 24 h after the first TNCB challenge (uptake ratio for treated ear to untreated ear, 1.02 ± 0.01). Repeated challenges with TNCB caused chronic inflammation, resulting in a steady increase in ^{125}I-gluco-RGD uptake (Fig. 5). After 13 challenges with TNCB, the ratio of tracer uptake of the treated ear to the untreated ear was 2.30 ± 0.27 ($P < 0.005$ compared with baseline; Fig. 5).

Increased tracer uptake of radiolabeled RGD peptide after repeated challenges with TNCB was also seen on PET imaging with ^{18}F-galacto-RGD (Fig. 6). In untreated mice, the ears were not seen in the PET images. After 1 challenge, only minimal tracer uptake in the treated ear was visible

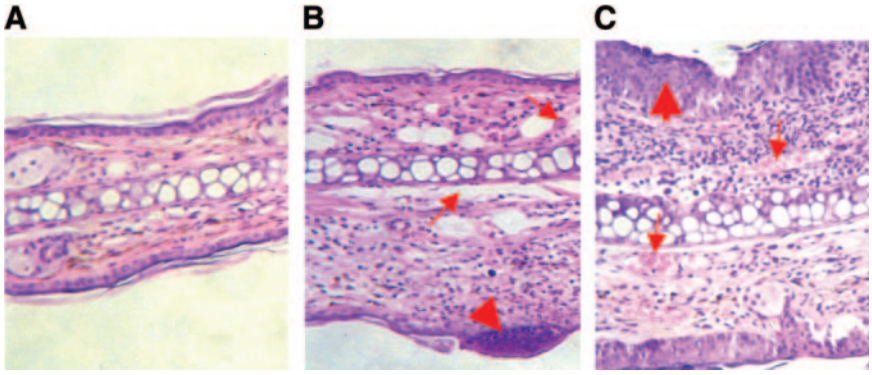

FIGURE 2. Hematoxylin- and eosin-stained ear sections of control mouse (A) and TNCB-sensitized mice (B and C) show morphologic changes 12 h after a single TNCB challenge (B) and after 10 challenges (C). B and C show, respectively, acute and chronic contact hypersensitivity reactions. Thick arrow in B indicates infiltrates by polymorphonuclear leukocytes and lymphocytes; thin arrows indicate dilated vessels. Thick arrow in C indicates epidermal hyperplasia and hyperkeratosis; thin arrows indicate blood vessels.

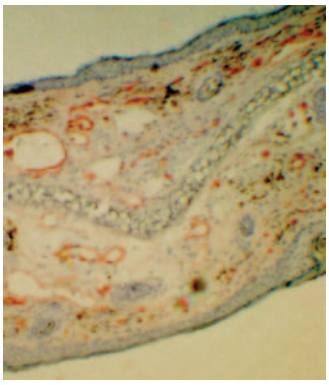

FIGURE 3. CD31 immunohistochemistry of ear section 12 h after 10th TNCB challenge demonstrates extensive neovascularization.

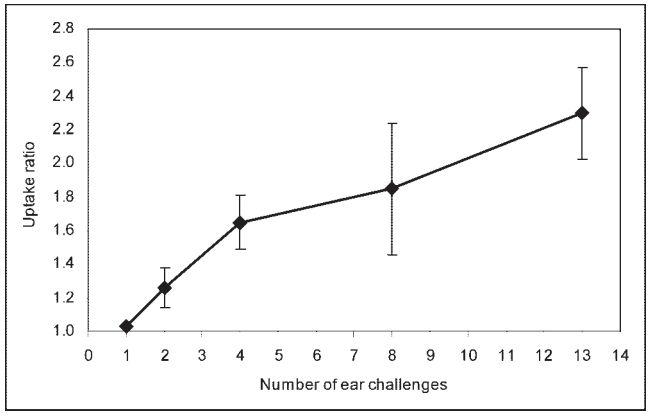

FIGURE 5. Time course of ^{125}I-gluco-RGD uptake ratio of challenged right ear and nonchallenged left ear versus number of challenges. Error bars denote 1 SD.

(Fig. 6A). However, after 10 challenges there was marked focal uptake of ^{18}F-galacto-RGD in the treated ear. The intensity of tracer uptake was about 4.7 times higher in the challenged right ear than in the untreated ear (Fig. 6B). Most important, when mice were intravenously injected with nonradiolabeled c(RGDfV), 18 mg/kg, 10 min before injection of ^{18}F-galacto-RGD, tracer uptake by the challenged ear could be reduced to background levels (Fig. 6C), confirming the specificity of ^{18}F-galacto-RGD uptake.

DISCUSSION

We used a TNCB-induced CHSR as a model to study $\alpha_v\beta_3$ integrin expression during acute and chronic inflammatory processes. CHSR can be divided into a sensitization phase, which is the priming of specific interferon-γ–producing T helper 1 and cytotoxic T lymphocyte cells, and an elicitation phase, which is the induction of T cell–mediated inflammation. Sensitization requires application of a hapten, such as TNCB, in combination with an irritant, such as acetone, to activate epidermal Langerhans' antigen-presenting cells. Activated hapten TNCB-carrying Langerhans' cells then traffic through afferent lymphatic vessels of the dermis to the draining axillary and inguinal lymph nodes. Inside the paracortical lymph node area, Langerhans' cells attract T cells and present hapten to the T cells, inducing TNCB-specific T cell activation and 1,000- to 100,000-fold T cell proliferation. These activated TNCB-specific T helper 1 and T lymphocyte cells can then migrate from the lymph nodes into the bloodstream.

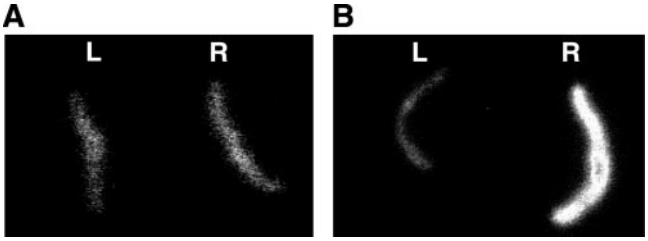

FIGURE 4. Typical autoradiograms of 20-μm sections from left (L) and right (R) mouse ears. (A) TNCB-sensitized mouse after first TNCB challenge (acute contact hypersensitivity). (B) TNCB-sensitized mouse after 10th challenge with TNCB.

Seven days after the initial sensitization, specific CHSR can be elicited by exposure of TNCB in a nonirritant oil solution on the right ear. This second TNCB exposure, the "challenge," attracts and activates the TNCB-specific T helper 1 and T lymphocyte cells at the site of challenge. This process is associated with rapid proliferation of TNCB-specific T helper 1 and cytotoxic T lymphocyte cells and cytokine production, specifically of interleukin-2, interferon-γ, and tumor necrosis factor (*13*), inducing a cascade of events that involve stimulation of multiple other cell types, including polymorphonuclear leukocytes, endothelial cells, mast cells, and keratinocytes (*20,21*).

Repeated exposure to TNCB at the same site induces a chronic inflammatory response associated with downregulation of interferon-γ production and upregulation of interleukin-4 production (*13,22*). The chronic TNCB-specific inflammatory process is accompanied by dense cellular infiltration, marked neovascularization, and a continuous increase in ear thickness due to acanthosis, hyperkeratosis, and interstitial edema.

Angiogenesis is a typical component of chronic CHSR. Several studies have shown expression of vascular endothelial growth factor and its receptors during the elicitation phase of CHSR (*23*). Blood vessels in chronic CHSR are dilated and demonstrate increased permeability to macromolecules, typical features of angiogenesis (*24*). Knockout mice lacking the angiogenesis inhibitor thrombospondin show more intense and prolonged CHSR reactions (*25*). In our study, increased microvessel density in the skin of the repeatedly challenged ear was documented by immunohistochemistry. Involvement of the $\alpha_v\beta_3$ integrin was determined using radiolabeled glycosylated RGD peptides. It has already been shown that this class of tracer allows noninvasive determination of $\alpha_v\beta_3$ expression in murine tumor models (*15,16*) and in patients (*17*). Therefore, the accumulation of RGD peptides observed in our study most likely reflects $\alpha_v\beta_3$ expression on activated endothelial cells during angiogenesis. In mice, however, immunohistochemical

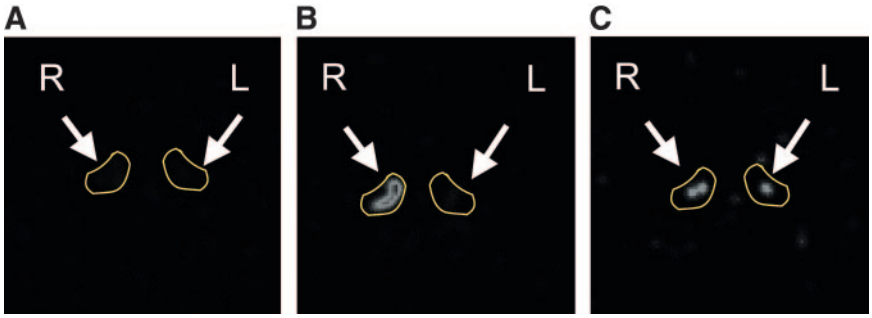

FIGURE 6. High-resolution PET images of challenged right ear and nonchallenged left ear with ^{18}F-galacto-RGD. Images are of mouse after 1 challenge (A), after 10 challenges (B), and after 10 challenges and blocking of $\alpha_v\beta_3$-receptors with unlabeled c(RGDfV) peptide, 18 mg/kg (C).

staining of the $\alpha_v\beta_3$ integrin is not feasible because of the lack of specific antibodies directed against murine $\alpha_v\beta_3$. Because $\alpha_v\beta_3$ can also be expressed on activated macrophages, lymphocytes, and granulocytes (*26,27*), we cannot fully exclude that the uptake of gluco- or galacto-RGD in chronic CHSR was also caused by accumulation in these cell types. However, tracer uptake was significantly greater in the treated ear than in the untreated ear only after the third challenge with TNCB. In contrast, histologic evaluation had already demonstrated dense leukocyte infiltrates 12 h after the first challenge, suggesting that $\alpha_v\beta_3$ expression by leukocytes is not a major factor for RGD uptake in CHSR.

Inflammatory processes may cause nonspecific uptake of numerous radiopharmaceuticals. This effect is due to regional increases in blood flow, vascular permeability, and extracellular volume (*28*). Therefore, it is particularly important to assess the specificity of tracer uptake in inflammatory processes. Two findings of our study indicated that uptake of gluco- and galacto-RGD was not due to unspecific mechanisms but to specific binding to the $\alpha_v\beta_3$ integrin. First, we did not observe increased uptake of gluco- or galacto-RGD in the acute phase of CHSR, although this phase is characterized by a marked increase in vascular permeability and edema formation. This finding suggests that unbound peptides had been washed out of the inflamed tissue by the time the imaging was performed. Second, tracer uptake in the chronic phase of CHSR was nearly completely blocked by pretreatment with an $\alpha_v\beta_3$ antagonist, confirming the receptor-specific tracer accumulation.

Because of the thinness of the normal mouse ear, the tracer uptake ratio calculated from the PET studies was clearly influenced by partial-volume effects: Tracer uptake in the treated ear might be overestimated relative to the untreated ear, because the treated ear is up to 5 times thicker than the untreated ear. However, we observed a significant difference in tracer uptake between the treated and untreated ears not only in the PET studies but also in autoradiograms of cryosections of identical thickness. Therefore, the possibility that the increased tracer accumulation found in the chronic CHSR is simply due to partial-volume effects can be excluded. Hence, our study indicated that radiolabeled RGD peptides specifically accumulate in the chronic inflamed tissue because of receptor-specific binding and that this process can be monitored noninvasively by PET.

CONCLUSION

Our data indicate that PET imaging with ^{18}F-galacto-RGD may be used to evaluate $\alpha_v\beta_3$ expression in inflammatory disorders and may represent a new biomarker for disease activity and for the monitoring of therapeutic interventions. In addition, this study showed, for what is to our knowledge the first time, that PET with radiolabeled RGD peptides might be a powerful tool to distinguish between acute and chronic T cell–mediated immune responses. Thus, further clinical studies of galacto-RGD for imaging of inflammatory processes in humans appear to be justified.

ACKNOWLEDGMENTS

The authors thank Claudia Bodenstein, Wolfgang Linke (Nuklearmedizinische Klinik der Technischen Universität München), Dagmar Dick, Sebastian Harrasser, and Doris Jakob (Department of Dermatology, Ludwig-Maximilians-University, Munich) for excellent technical support. The work was supported by Wilhelm-Sander-Stiftung (97.041.2) and the Deutsche Krebshilfe (10-1917).

REFERENCES

1. van der Flier A, Sonnenberg A. Function and interactions of integrins. *Cell Tissue Res.* 2001;305:285–298.
2. Eliceiri BP, Cheresh DA. The role of alpha(v) integrins during angiogenesis: insights into potential mechanisms of action and clinical development. *J Clin Invest.* 1999;103:1227–1230.
3. Plow EF, Haas TA, Zhang L, Loftus J, Smith JW. Ligand binding to integrins. *J Biol Chem.* 2000;275:21785–21788.
4. Xiong JP, Stehle T, Zhang R, et al. Crystal structure of the extracellular segment of integrin alpha(v)beta(3) in complex with an Arg-Gly-Asp ligand. *Science.* 2002;296:151–155.
5. Haubner R, Finsinger D, Kessler H. Stereoisomeric peptide libraries and peptidomimetics for designing selective inhibitors for alpha(v)beta(3) integrins for a new cancer therapy. *Angew Chem Int Ed Engl.* 1997;36:1374–1389.
6. Haubner RH, Wester HJ, Weber WA, Schwaiger M. Radiotracer-based strategies to image angiogenesis. *Q J Nucl Med.* 2003;47:189–199.
7. Christofidou-Solomidou M, Bridges M, Murphy GF, Albelda SM, DeLisser HM. Expression and function of endothelial cell alpha(v) integrin receptors in wound-induced human angiogenesis in human skin/SCID mice chimeras. *Am J Pathol.* 1997;151:975–983.
8. Bishop GG, McPherson JA, Sanders JM, et al. Selective alpha(v)beta(3)-receptor blockade reduces macrophage infiltration and restenosis after balloon angioplasty in the atherosclerotic rabbit. *Circulation.* 2001;103:1906–1911.
9. Pablos JL, Santiago B, Galindo M, et al. Synoviocyte-derived CXCL12 is displayed on endothelium and induces angiogenesis in rheumatoid arthritis. *J Immunol.* 2003;170:2147–2152.
10. Creamer D, Allen M, Sousa A, Poston R, Barker J. Altered vascular endothelium integrin expression in psoriasis. *Am J Pathol.* 1995;147:1661–1667.
11. Storgard CM, Stupack DG, Jonczyk A, Goodman SL, Fox RI, Cheresh DA.

Decreased angiogenesis and arthritic disease in rabbits treated with an alphavbeta3 antagonist. *J Clin Invest.* 1999;103:47–54.
12. Wilder RL. Integrin alpha V beta 3 as a target for treatment of rheumatoid arthritis and related rheumatic diseases. *Ann Rheum Dis.* 2002;61(suppl 2):ii96–ii99.
13. Kitagaki H, Ono N, Hayakawa K, Kitazawa T, Watanabe K, Shiohara T. Repeated elicitation of contact hypersensitivity induces a shift in cutaneous cytokine milieu from a T helper cell type 1 to a T helper cell type 2 profile. *J Immunol.* 1997;159:2484–2491.
14. Ross R, Reske-Kunz AB. The role of NO in contact hypersensitivity. *Int Immunopharmacol.* 2001;1:1469–1478.
15. Haubner R, Wester H-J, Burkhart F, et al. Glycosylated RGD-containing peptides: tracer for tumor targeting and angiogenesis imaging with improved biokinetics. *J Nucl Med.* 2001;42:326–336.
16. Haubner R, Wester H-J, Weber WA, et al. Noninvasive imaging of $\alpha_v\beta_3$ integrin expression using ^{18}F-labeled RGD-containing glycopeptide and positron emission tomography. *Cancer Res.* 2001;61:1781–1785.
17. Beer AJ, Haubner R, Essler M, et al. Non-invasive imaging of αvβ3-expression with F-18-galacto-RGD and PET: initial results in patients [abstract]. *J Nucl Med.* 2004;45(suppl):192P.
18. Haubner R, Kuhnast B, Mang C, et al. [^{18}F]galacto-RGD: synthesis, radiolabeling, metabolic stability, and radiation dose estimates. *Bioconjugate Chem.* 2004; 15:61–69.
19. Ziegler SI, Pichler BJ, Boening G, et al. A prototype high-resolution animal positron tomograph with avalanche photodiode arrays and LSO crystals. *Eur J Nucl Med.* 2001;28:136–143.
20. Biedermann T, Kneilling M, Mailhammer R, et al. Mast cells control neutrophil recruitment during T cell-mediated delayed-type hypersensitivity reactions through tumor necrosis factor and macrophage inflammatory protein 2. *J Exp Med.* 2000;192:1441–1452.
21. Krasteva M, Kehren J, Ducluzeau MT, et al. Contact dermatitis I: pathophysiology of contact sensitivity. *Eur J Dermatol.* 1999;9:65–77.
22. Kitagaki H, Fujisawa S, Watanabe K, Hayakawa K, Shiohara T. Immediate-type hypersensitivity response followed by a late reaction is induced by repeated epicutaneous application of contact sensitizing agents in mice. *J Invest Dermatol.* 1995;105:749–755.
23. Zhang N, Fang Z, Contag PR, Purchio AF, West DB. Tracking angiogenesis induced by skin wounding and contact hypersensitivity using a Vegfr2-luciferase transgenic mouse. *Blood.* 2004;103:617–626.
24. Dieli F, Sireci G, Scire E, Salerno A, Bellavia A. Impaired contact hypersensitivity to trinitrochlorobenzene in interleukin-4-deficient mice. *Immunology.* 1999; 98:71–79.
25. Lange-Asschenfeldt B, Weninger W, Velasco P, et al. Increased and prolonged inflammation and angiogenesis in delayed-type hypersensitivity reactions elicited in the skin of thrombospondin-2-deficient mice. *Blood.* 2002;99:538–545.
26. Maxfield SR, Moulder K, Koning F, et al. Murine T cells express a cell surface receptor for multiple extracellular matrix proteins: identification and characterization with monoclonal antibodies. *J Exp Med.* 1989;169:2173–2190.
27. Sixt M, Hallmann R, Wendler O, Scharffetter-Kochanek K, Sorokin LM. Cell adhesion and migration properties of beta 2-integrin negative polymorphonuclear granulocytes on defined extracellular matrix molecules: relevance for leukocyte extravasation. *J Biol Chem.* 2001;276:18878–18887.
28. Becker W, Meller J. The role of nuclear medicine in infection and inflammation. *Lancet Infect Dis.* 2001;1:326–333.

JNM The Journal of NUCLEAR MEDICINE

Imaging of Delayed-Type Hypersensitivity Reaction by PET and ^{18}F-Galacto-RGD

Bernd J. Pichler, Manfred Kneilling, Roland Haubner, Heidi Braumüller, Markus Schwaiger, Martin Röcken and Wolfgang A. Weber

J Nucl Med. 2005;46:184-189.

The Journal of Nuclear Medicine is published monthly.
SNMMI | Society of Nuclear Medicine and Molecular Imaging
1850 Samuel Morse Drive, Reston, VA 20190.
(Print ISSN: 0161-5505, Online ISSN: 2159-662X)

SNMMI SOCIETY OF NUCLEAR MEDICINE AND MOLECULAR IMAGING